

Soft x-ray submicron imaging detector based on point defects in LiF

G. Baldacchini, S. Bollanti, F. Bonfigli, F. Flora,^{a)} P. Di Lazzaro, A. Lai, T. Marolo, R. M. Montereali, and D. Murra

ENEA, Department of FIS-ACC, C.R. Frascati, Via E. Fermi 45, 00044 Frascati, Rome, Italy

A. Faenov and T. Pikuz

Multicharged Ions Spectra Data Center of VNIIFTRI, Mendeleevo, Moscow Region, 141570, Russia

E. Nichelatti

ENEA, Department of FIS-OTT, C.R. Casaccia, Via Anguillarese 301, 00060 S.Maria di Galeria, Rome, Italy

G. Tomassetti, A. Reale, L. Reale, and A. Ritucci

INFN and Dipartimento di Fisica dell'Università dell'Aquila and LNGS-INFN, Assergi (L'Aquila), Italy

T. Limongi and L. Palladino

INFN and Dipartimento di Biologia dell'Università dell'Aquila and LNGS-INFN, Assergi (L'Aquila), Italy

M. Francucci, S. Martellucci, and G. Petrocelli

INFN and Università di Roma Tor Vergata, Via del Politecnico, n. 1, 00173 Rome, Italy

(Received 19 May 2005; accepted 3 October 2005; published online 17 November 2005)

The use of lithium fluoride (LiF) crystals and films as imaging detectors for EUV and soft-x-ray radiation is discussed. The EUV or soft-x-ray radiation can generate stable color centers, emitting in the visible spectral range an intense fluorescence from the exposed areas. The high dynamic response of the material to the received dose and the atomic scale of the color centers make this detector extremely interesting for imaging at a spatial resolution which can be much smaller than the light wavelength. Experimental results of contact microscopy imaging of test meshes demonstrate a resolution of the order of 400 nm. This high spatial resolution has been obtained in a wide field of view, up to several mm². Images obtained on different biological samples, as well as an investigation of a soft x-ray laser beam are presented. The behavior of the generated color centers density as a function of the deposited x-ray dose and the advantages of this new diagnostic technique for both coherent and noncoherent EUV sources, compared with CCDs detectors, photographic films, and photoresists are discussed. © 2005 American Institute of Physics.

[DOI: [10.1063/1.2130930](https://doi.org/10.1063/1.2130930)]

I. INTRODUCTION

The possibility of detecting images in the extreme ultraviolet (EUV) and soft x-ray spectral range (photon energies $h\nu \cong 20\text{--}8000$ eV), at a high spatial resolution and on a wide field of view is considered a topical task nowadays. Indeed, the fast development of different types of EUV and soft x-ray sources (laser produced plasmas, synchrotron radiation, x-ray lasers) makes its application very attractive in the different physical science, material science, and biomedical investigations.^{1–5}

In the EUV and soft x-ray imaging applications, three types of detectors have been used up to now: x-ray photographic films,⁶ photoresists,⁷ and charge coupled devices (CCDs),⁸ but each of them has advantages and drawbacks at the same time.

The main advantages of the x-ray films are a reasonable spatial resolution (of the order of few microns), a very big size of detection areas (many cm² could be easily used), and a low price. However, their typical dynamic range is rather

low (in the range of 5–8 bits); moreover, it is necessary to develop the films after irradiation and then to digitize them in order to obtain interesting biological or physical data. So, their response is far from being a real-time one.

On the contrary, x-ray CCDs are very efficient detection devices thanks to their extremely high sensitivity (single photons can be detected by means of coupling with image intensifiers), to their high dynamic range (10–16 bits), and to the simplicity in their readout process, which allows to obtain experimental data in real time (the dynamic range is defined as the number of bits, n , referring to the amount of tonalities, 2^n , between white and black which can be observed). But, as a drawback their spatial resolution is presently limited typically to 4 microns, so that in order to decrease this value the images should be magnified onto the CCD through an x-ray optical system, like a zone-plate lens, i.e., the so-called projection mode. Moreover, their sensitive area is just of the order of 1–10 cm², and the prices are very high. Finally, when using projection optics, even the soft x-ray source becomes expensive. Indeed, zone plate lenses require monochromatic radiation, and the high fluence on the

^{a)} Author to whom correspondence should be addressed; electronic mail: flora@frascati.enea.it

sample (needed for a high resolution, that is for a low statistical noise) can be achieved only by using high spectral brightness sources, like the synchrotron one.

Remaining in the simpler imaging technique called "contact mode," when a submicron resolution of the image is needed (in x-ray contact microscopy and in microradiography, or in x-ray focusing experiments), photoresist-based detectors, like, for example, the well known Poly-Methyl-MetAcrilate (PMMA) photoresist are commonly used.⁷ These detectors reach a very high spatial (about 10 nanometer-scale) resolution, but they require a relatively high-energy density of illumination (≥ 2 mJ/cm², depending on the quality of resolution), and they have a very poor dynamic range (just 5–6 bits for PMMA). After exposure, they need a development process and a further complicated and time-consuming data acquisition reading through an Atomic Force Microscope (AFM), which practically does not permit to analyze images with a field of view larger than few tenths of mm².

So, the search for a high-dynamic-range and cheap detector for EUV and soft x-ray radiation, which at the same time produces images with nanometer scale spatial resolution in a large field of view requiring a reasonably simple procedure, short data acquisition and processing time, is of paramount importance.

A very promising candidate as submicron resolution x-ray detector is lithium fluoride (LiF) in the form of crystal and film. It is well known that LiF, as other alkali halide crystals, can host different types of stable color centers (CCs) produced under bombardment by ionizing radiation, like high energy photons and elementary particles (gamma and hard x-rays, neutrons, electrons, and ions).⁹ Under optical excitation by properly selected pumping light, several types of CCs in LiF emit light in the visible spectral range even at room temperature (RT). Since the dimension of the single CC is less than 1 nm,¹⁰ and the CCs concentration can reach values of the order of 10^{19} – 10^{20} cm⁻³, two-dimensional images with high spatial resolution (much smaller than 1 micron) can be generated by ionizing radiation in LiF material.

Low-energy electron^{11–13} or ion beams¹⁴ are commonly used for direct writing of colored tiny structures in LiF. For example, submicron luminescent patterns down to a width of 0.1 μ m have been obtained by using an electron beam encoding technique¹¹ in a LiF crystal and in a LiF film.¹² With electron-beam irradiation the spatial resolution is limited by the beam broadening due to charge effects in insulating materials, and also by lateral spreading of the electrons due to scattering processes in the interaction volume. Moreover, this technique can produce only small colored areas at the price of rather long exposure time (\sim some days/cm² when using electron beams with a current value around 2 nA). On the other hand, highly penetrating radiations, like gamma and hard x-ray beams, are not suitable either to color thin layers with controlled depth and to produce colored areas with high spatial resolution (in this case the resolution is limited by photoelectron blurring, as it is well known in proximity x-ray lithography experiments¹⁵). On the contrary, the low penetration depth of soft x-rays and EUV light make both these

types of electromagnetic radiation very attractive for coloration of LiF in a relatively short exposure time.

In this article the use and characterization of LiF (in the form of bulk crystals or films grown on different substrates) as a high-resolution, large-field of view imaging detector in the spectral range of EUV and soft x-ray radiation is presented.

II. SOFT X-RAY IMAGING DETECTORS BASED ON LiF

A. Principles of LiF coloration

As in the other alkali halide crystals, photons with energy greater than the band-gap separation produce different types of CCs in LiF crystals and films. However, there are some features, which make LiF a unique material as far as coloration is concerned:

- (i) Several CCs generated in LiF are stable at RT, which is very important for various applications;
- (ii) The band gap is about 14 eV, which is the largest among all other alkali halides or dielectric materials. This means that CCs can not be easily generated by visible and near UV radiation (unless at extremely high intensities and involving multiphoton absorption processes), so that a LiF based detector does not require any filter for protection from such radiation;
- (iii) The cation-anion distance is the shortest for LiF crystals, and the Li⁺ and F⁻ ions possess the smallest radius among the alkali and halide ions, respectively. This means that the CCs density can reach very high values, and the highest spatial resolution could be obtained using this material;
- (iv) LiF can be deposited as a film by thermal evaporation on different substrates. In this case LiF assumes a polycrystalline structure and, as it will be shown below, the formation efficiency of CCs is higher than in bulk LiF crystals. This implies an increasing in sensitivity of imaging detector for soft x-ray radiation;
- (v) LiF crystal hosts optically active CCs with absorption bands (photon energy of the pumping radiation) and emission bands (photon energy of luminescence) in the visible spectral range. This allows a strongly simplified readout procedure, through the use of commercially available high-resolution optical or confocal fluorescence microscopes;
- (vi) Notwithstanding CCs in LiF are stable at RT (as a matter of fact, up to ~ 120 °C), they can be easily destroyed at temperature >400 °C.¹⁶ After cooling down, LiF can be colored again. This means that, in practice, LiF detectors could be used as rewritable devices;
- (vii) Finally, LiF crystals are commercially available (they are relatively cheap optical materials) in the form of big-size crystal plates with high surface quality.

At RT, ionizing radiation in LiF generates different types of CCs simultaneously, but only F₂ and the F₃⁺ CCs have a practical interest in our case, because they mainly contribute for visible photoluminescence. The F-center [see Fig. 1(a)], consisting of an anion vacancy occupied by an electron, is

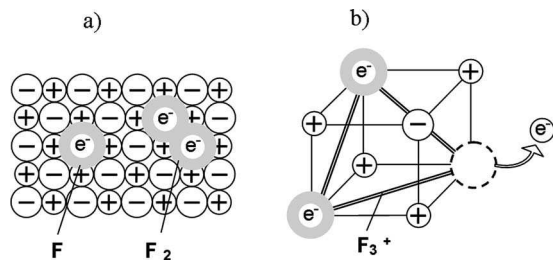


FIG. 1. (a) F-type CCs in alkali halide crystals. If one electron replaces an anion vacancy generated by ionizing radiation, a primary F-center is created. If two primary F centers aggregate, an F_2 color center is obtained; (b) If in a three aggregated primary centers (that is an F_3 color center) one electron is missed, the center is called F_3^+ .

the simplest and primary defect appearing in LiF under ionizing radiation. The concentration of the primary F-centers plays a crucial role in the formation of more complex aggregates of CCs, and in particular of the F_2 and F_3^+ centers^{17,18} [see Figs. 1(a) and 1(b)], which consist of two electrons bound to two and three close anion vacancies, respectively. It is worthwhile noticing that, although investigations started a long time ago,¹⁹ up to now no fluorescence unambiguously originating from the F-centers in LiF has been detected.²⁰ At the same time, for practical applications, the main advantages of F_2 and F_3^+ CCs derive from their photoemissions in the visible spectral range¹⁹ and gain coefficients as high as a few cm^{-1} .²¹ Moreover, they have almost overlapping absorption bands peaked at ~ 450 nm (see Fig. 2) and, therefore, they can be simultaneously excited by a single pumping wavelength.^{20–22}

The previous electronic defects are particularly interesting for the LiF application as x-ray detector, because they are efficiently created by low penetrating ionizing radiation and, under blue-light pumping, they efficiently emit light in the visible spectral range, with higher efficiency than other more complex generated CCs. In conclusion, despite the fact that

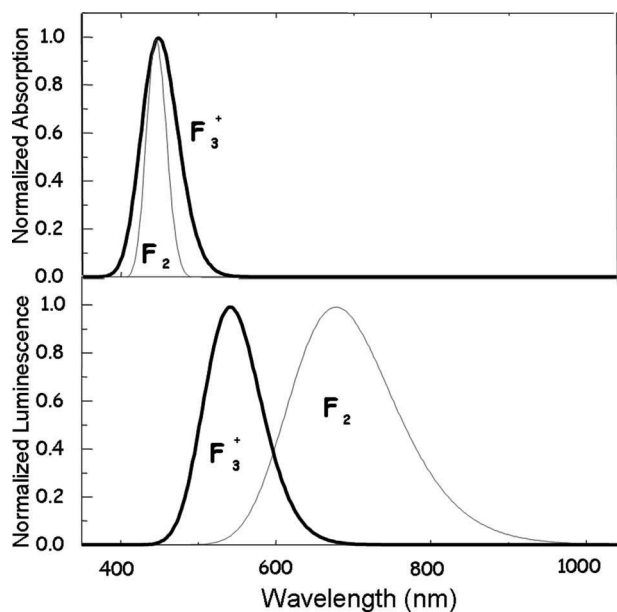


FIG. 2. Normalized absorption (top) and emission (bottom) bands of F_2 and F_3^+ color centers in LiF at RT.

more complex defects could appear under soft x-ray irradiation of LiF crystals, only the F_2 and F_3^+ CCs are worth analyzing for understanding the principles of x-ray images formation in LiF. The intensity of CCs photoluminescence depends on the concentration of F_3^+ and F_2 centers generated in the irradiated LiF material. As F_2 and F_3^+ CCs are aggregated from primary F-centers, their concentration in LiF crystals is related to the efficiency of the primary F-centers generation. This means that the sensitivity of LiF, as a soft x-ray imaging detector, strongly depends on the possibility of producing such centers with high efficiency inside the material. According with the experimental data reported in Ref. 9, for alkali halides (in NaCl crystals for example) colored with hard x-rays, the concentration of the primary F centers seems to increase roughly as the square root of the irradiation dose D (D is the soft x-ray energy deposited per unit volume) and with the logarithm of the dose rate $P = dD/dt$ (P is the rate of soft x-ray energy deposition per unit volume).

The intensity of photoluminescence is proportional to the intensity of the excitation pumping beam below saturation. In entirely colored LiF crystals irradiated by 5 MeV electrons, under continuous blue radiation pumping, the luminescence increases linearly with the concentration of the F_3^+ and F_2 centers up to $\sim 10^{16}$ centers/ cm^3 and $\sim 10^{18}$ centers/ cm^3 , respectively.²² With further increasing the CCs density, up to 10^{20} CCs/ cm^3 , the luminescence undergoes a saturation effect²² and the emission efficiency decreases.

B. Operation of LiF based soft x-ray imaging detectors

The principle of operation of the LiF based soft x-ray imaging detector consists of two steps. As a first step, the surface of the LiF detector is exposed to x-ray radiation, which generates CCs, whose density depends on the x-ray absorbed dose. Any x-ray source, such as laser-produced plasma (LPP), x-ray tube, x-ray laser, synchrotron radiation and so on, can be used. As seen in the former section, larger is the dose rate deposited, higher is the coloration efficiency achieved. Figure 3(a) (above) shows a LPP for contact imaging on LiF. A laser beam is focused on a target and creates a high temperature plasma, which practically radiates uniformly in a 2π solid angle in the wavelength spectral range below the LiF band gap. Downstream of the plasma radiation, the object under study and a LiF detector are placed close each other. The x-ray radiation, attenuated by the object, produces on the LiF detector CCs, whose density is proportional to the intensity of the radiation transmitted through the same object. So, an image formed by different CC densities is stored on the LiF surface. In the case of a directional x-ray beam (for example, x-ray laser beam, synchrotron radiation), the LiF detector could be used to record the intensity distribution of the x-ray radiation itself or as an object transmission map at projection mode (pos.1) or contact mode (pos.2), see Fig. 3(a) below.

As a second step, the readout process is performed as in Fig. 3(b). For the observation of the luminescent image stored in the LiF detector, optical microscopes operating in fluorescence mode are used. The x-ray irradiated LiF sample

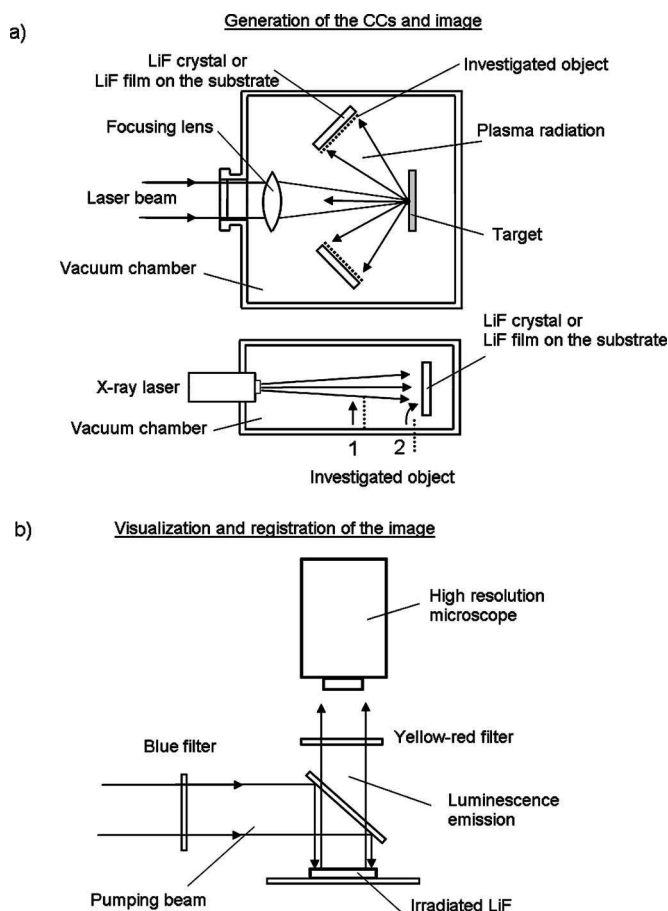


FIG. 3. Principle of LiF detector operation: (a) first step-irradiation of LiF by soft x-ray beam (above in case of the LPP radiation and below in case of direct x-ray beam); (b) second step-readout process of the irradiated LiF samples by optical microscope operating in the fluorescence mode.

is excited by light in the blue spectral range and the emitted photoluminescence is observed in the yellow-red visible interval, where the broad emission bands of the F_2 and F_3^+ centers are located. Generally, the spatial resolution is limited by the readout process of the irradiated LiF surface, rather than the irradiation imprinting. In other words, the final spatial resolution of such imaging detector is generally limited by the performances of the optical microscope. For a conventional one the limit is around $0.5\text{--}0.6\ \mu\text{m}$, for an optical confocal microscope the lateral spatial resolution can be around $0.2\ \mu\text{m}$, while a scanning near-field optical microscope (SNOM) can reach resolution values much smaller than the light wavelength.

C. Properties of LiF imaging detectors by using soft x-ray radiation of laser-produced-plasma sources

1. X-ray sources

In this work, for the characterization of LiF crystals and films as x-ray imaging detectors, a laser produced plasma with enough intensity of EUV and x-ray radiation for coloration has been used. Most of the experiments were carried out at the ENEA Hercules laser facility²³ in Frascati, Italy, which possesses a XeCl excimer laser with an active volume of $(9 \times 5 \times 100)\ \text{cm}^3$ and emission at $0.308\ \mu\text{m}$. A laser beam

energy of $0.5\text{--}1\ \text{J}$ with a $10\ \text{ns}$ pulse duration at a repetition rate of $0.5\ \text{Hz}$ was used. The laser radiation was focused by a triplet lens on solid Cu or Fe tape targets to form a spot of $30\ \mu\text{m}$ in diameter. Thus, the laser intensity on the target was about $0.5\text{--}1 \times 10^{13}\ \text{W}/\text{cm}^2$, resulting to a plasma electron temperature of $150\text{--}200\ \text{eV}$. Such a Fe or Cu plasma emits soft x-rays mainly in the energy range $0.05\text{--}1.5\ \text{keV}$.²³

Some experiments were carried out at Tor Vergata University of Rome, Italy, where the plasma was produced using the fundamental output wavelength of a Nd:glass laser. The laser source was a Quantel Nd:glass laser delivering pulses with a maximum energy of $10\ \text{J}$ and a temporal duration of $12\ \text{ns}$. It consisted of a chain of two Nd:YAG and two Nd:glass amplifiers. The repetition rate was limited to $1\ \text{shot}/\text{min}$ to minimize the thermal lens effect. A $20\ \text{cm}$ focal-length doublet lens focused the laser beam onto a solid Cu tape target. The estimated beam diameter at the focal point was $200\ \mu\text{m}$, with a corresponding laser intensity on the target of about $10^{12}\ \text{W}/\text{cm}^2$. The obtained plasma mainly radiated in the energy range $0.05\text{--}2\ \text{keV}$.²⁴

2. Coloration efficiency of LiF crystals and films by soft x-ray

In order to characterize the efficiency of CCs formation in LiF crystals under soft x-ray irradiation, the upper scheme shown in Fig. 3(a) has been used. In this work we have considered as imaging detectors LiF crystals and polycrystalline films. The first ones are commercially available, while the last ones have been produced at the ENEA Laboratory in Frascati, Italy. The used LiF films have been grown on silicon or glass substrates by a thermal evaporation technique. Their structural, morphological and optical properties have been summarized elsewhere,²⁵ while their thickness could be varied from 0.05 up to $6\ \mu\text{m}$.

A comparison of the coloration efficiency by EUV and soft x-rays of a LiF crystal and a LiF film has been performed as in the following. A LiF film with a thickness of $\sim 6\ \mu\text{m}$ grown on a glass substrate kept at $250\ ^\circ\text{C}$ during the deposition and a LiF crystal $2\ \text{mm}$ thick were placed at a distance of $10\ \text{cm}$ from the XeCl-laser plasma x-ray source under an angle of about 20° from the normal to the source target. Both LiF samples were oriented perpendicularly to the incident x-ray radiation, with an irradiated area of $(6 \times 7)\ \text{mm}^2$, and were exposed to 780 shots. According to previous data,²³ the XeCl laser radiation has an average conversion efficiency of about 20% in part of the EUV and soft x-ray energy spectral region. So, including the triplet lens transmission value, at the distance of $10\ \text{cm}$ from the x-ray source a flux density of $\sim 0.4\ \text{mJ}/\text{cm}^2/\text{shot}$ is expected. The measured RT emission spectra of the colored LiF film and LiF crystal, both exposed at an x-ray fluence of $\sim 300\ \text{mJ}/\text{cm}^2$, excited with the $458\ \text{nm}$ line of Ar laser at the same pumping power intensity (about few mW/cm^2), are presented in Fig. 4. The photoluminescence spectra, corrected for the detection system optical response, consist of two broad bands, peaking at around 540 and $670\ \text{nm}$, which correspond to the well known positions of F_3^+ and F_2 centers, respectively.^{26,27} The maximum of the emission spectra is at around $670\ \text{nm}$ due to the F_2 CCs luminescence, as shown in

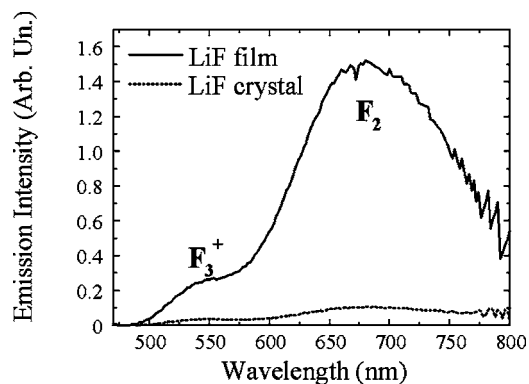


FIG. 4. Photoluminescence spectra at RT of a LiF crystal and a 6 μm thick polycrystalline LiF film, both exposed to EUV and soft x-rays at the same irradiation conditions.

Fig. 2, which is very convenient for the readout process because of the high sensitivity of light detectors in this spectral region. It is very important to stress here that a comparison of the photoluminescence spectra of LiF film and crystal, see Fig. 4, shows more than 10 times higher emission intensity for the LiF film than for the crystal. The reason for this result seems to be connected with the different structure of the film (polycrystalline) and the bulk crystal (monocrystalline),²⁷ as well as to their peculiar morphological structure.²⁵

In order to change the x-ray fluence, a LiF film was covered by a polypropylene step-shaped filter, which reduced the x-ray fluence from 6 to 30 times with respect to the open part, corresponding to a fluence of 600 mJ/cm^2 . The image was readout by a conventional optical microscope in fluorescence mode. A 458 nm ion Ar laser was used as pumping beam in the blue region and a proper glass optical filter was applied for the observation of the fluorescent image, as shown in Fig. 3(b). Figure 5 shows the image obtained on the LiF film. The strong photoluminescence of the areas corresponding to the full dose of x-ray radiation, and the different levels of luminescence from the other parts, are very well observed and distinguished.

A very important point for the characterization of the sensitivity of LiF crystals and films as soft x-ray imaging

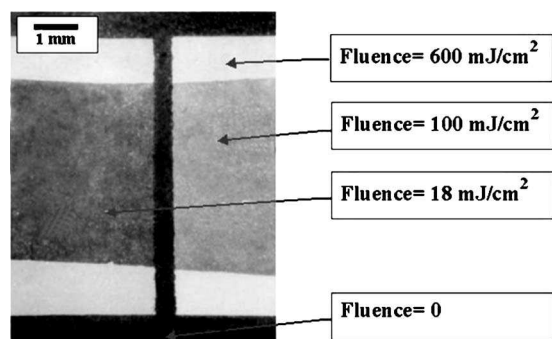


FIG. 5. LiF film sample exposed to approximately 9000 shots at 12 cm from the XeCl laser-plasma soft-x-ray source through a 0.8 μm Al filter (transmitting in the 40–72 eV EUV spectral range), followed by a polypropylene step-shaped filter; a fluence of 600 mJ/cm^2 is reached on the open area of the film, while a fluence zero is corresponding to the completely closed area of the film. The sample is observed in fluorescence mode by exciting at 458 nm with an ion Ar laser, and observing by a low magnification microscope through a yellow filter.

detectors is the determination of the photoemission dependence as a function of the soft x-ray irradiation dose. As it was described above, the visible emission efficiency of LiF directly depends from the concentration of F_2 and F_3^+ CCs. Since such CCs are created through the aggregation of primary F-centers, it means that the primary F-centers concentration establishes the efficiency of CCs generation and the sensitivity of a LiF crystal and film as soft-x-ray detector.

For the estimation of the LiF sensitivity, the optical characterization of irradiated LiF samples (absorption and emission spectral measurements) has been performed. According to the Smakula's formula,²⁸ which describes the relation between the absorption band spectral parameters and the CCs concentration, the densities of the generated CCs (under different conditions) were estimated. For example, in the case of 480 mJ/cm^2 irradiation fluence, the densities of the CCs in the colored LiF layer film were estimated to be $\sim 2.5 \times 10^{20} \text{ cm}^{-3}$ for F-centers and $\sim 1.5 \times 10^{19} \text{ cm}^{-3}$ for the ($\text{F}_2 + \text{F}_3^+$) centers.²⁹ As it has been shown in Ref. 9, generally for alkali halide crystals colored by hard x-rays the concentration of the primary F centers increases roughly as the square root of the irradiation dose D (i.e., energy deposited into unit of the media volume), and with the logarithm of the dose rate $P = dD/dt$. The experimental points reported in Ref. 9 for NaCl concerning the F centers concentration $f(D, P)$ vs the irradiation dose D and dose rate P are well fitted by the following empirical equation:

$$f(D, P) = k\sqrt{D} \left[1 + \log \left(1 + \frac{P}{P_s} \right) \right]^2, \quad (1)$$

where $P_s = 10 \text{ mJ cm}^{-3} \text{ s}^{-1}$ is the LiF threshold dose rate, above which nonlinear effects in the coloration process start to be important, $k = 7.7 \times 10^{15} \text{ J}^{-1/2} \text{ cm}^{-3/2}$ is the coefficient indicating the F-type CCs density given by a unit dose of 1 J/cm^3 at a deposition rate $P \leq P_s$, and k is constant for a given media.

Equation (1) shows that in order to reach a CCs density of $10^{18} - 10^{19} \text{ cm}^{-3}$ in the irradiated volume, it is very important to have either a suitable dose of deposited radiation, either a high value of the dose rate, i.e., a high rate of the energy deposition process. For this reason, plasma sources, created by interaction of short duration ($10^{-7} - 10^{-12} \text{ s}$) laser pulses with different targets are very efficient for generating CCs. Due to their high intensity and short emission time, the dose rate very easily could reach values up to few GW cm^{-3} , which will increase the density of CCs by one order of magnitude and reduce the time of the irradiation.

As shown in Ref. 30 and in Fig. 6, by exposing a LiF crystal to different EUV dose values (just by changing the number of shots of our EUV LPP source), we found out that the F centers concentration generated in LiF follows the same equation with the same parameter values within few percent, although the material has changed from NaCl to LiF, as well as the spectral range of the x-rays and the dose rate (by many orders of magnitude).

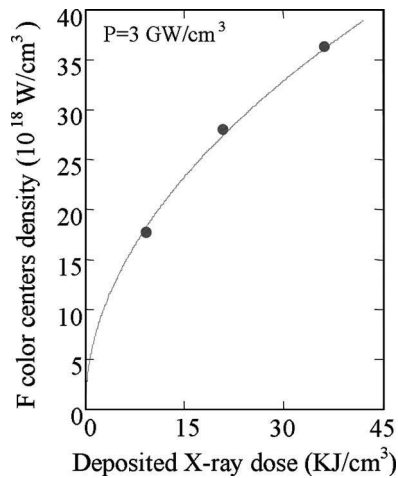


FIG. 6. F center density in LiF crystal as a function of the soft-x-ray irradiation doses D at a dose rate $P=3$ GW/cm³; the experimental data (dots) are well fitted by Eq. (1) for $k=8.0 \times 10^{15}$ J^{-1/2} cm^{-3/2} and $P_S = 10$ mW/cm³.

3. Spatial resolution of soft x-ray imaging detectors based on CCs in LiF

As it was mentioned above, one of the most important characteristics of soft-x-ray imaging detectors is their spatial resolution. In principle, the spatial resolution of LiF crystals and films is limited only by the size of the CCs, which is at the level of the atomic scale. The migration of CCs inside LiF is of the order of few lattice distances. It means that the spatial resolution of LiF based detectors could be at values around 1 nm. At the same time, as previously mentioned, the spatial resolution of the readout system could be limited also by the depth of penetration of the x-ray radiation inside the detector, just because high resolution microscopes are based on large numerical aperture objectives. The penetration depth of EUV and soft x-ray radiation (energy range 20–1500 eV) in LiF ranges from 20 nm up to few microns.⁶ So, it is expected that the limit of spatial resolution, which could be reached using LiF crystals or films as a soft x-ray imaging detector could be smaller than 100 nm in the EUV and few microns in the soft x-rays. Of course, in the case of LiF films, the depth of coloration, and consequently the resolution, can be limited by selecting the film thickness. However, the use of very thin LiF films could also reduce the efficiency of the detector when higher photon energies are used.

To check such predictions, some test experiments have been done using a soft x-ray plasma point source generated by XeCl or Nd glass laser pulses (see lasers parameter description above). A schematic of the experimental setup is shown in Fig. 3(a). In order to test the spatial resolution, in one of our first experiments a couple of copper meshes with a diameter of 3 mm (wire thickness 10 μ m, period 60 μ m) were mounted side by side in contact with a LiF crystal. So, the grids masked the crystal from the incoming radiation. This “sandwich” was placed inside the vacuum chamber at a distance of 15 cm from the XeCl laser produced plasma source. The large emission angle of the x-ray radiation from the source allowed us to expose the full surface of the detector, covered by the grids, in any single shot. The EUV and soft x-ray fluence was roughly 0.2 mJ/cm²/shot when using

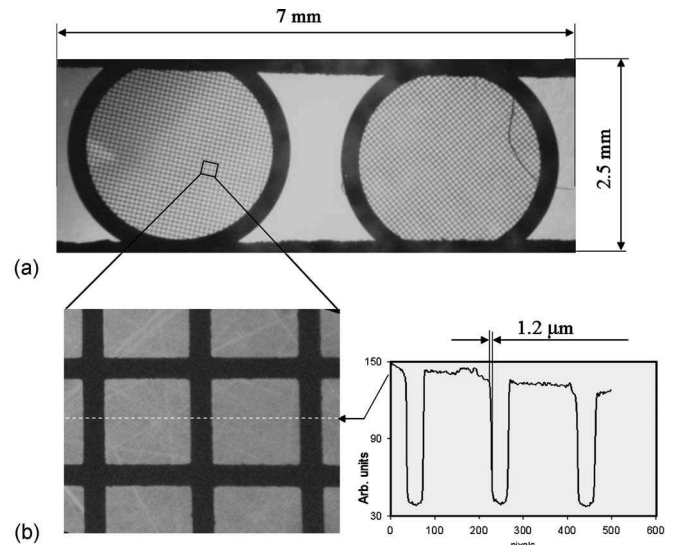


FIG. 7. (a) Image of grids (the diameter of the circles is 3 mm, the period is 60 μ m, the thickness of the wires is 10 μ m) on a LiF crystal, observed with an optical microscope in fluorescence mode with a 5 \times objective. The grids were placed in contact with the LiF crystal and irradiated by soft-x-ray radiation, created by interaction of the XeCl laser with a Fe target, in 1000 shots; (b) enlarged part of the image, observed with a Nikon microscope with a 40 \times objective; the densitogram of the image shows a spatial resolution value close to the spatial resolution limit of the microscope.

an iron target. In our experiments the target was irradiated by 1000 laser shots. The obtained image was readout by using an optical microscope in fluorescence mode, while the blue pump light was cut off with a colored-glass filter, as already explained.

Figure 7(a) shows the image of the luminescent patterns: the uncolored black parts represent the dark shadow of the grids, while the gray ones correspond to the luminescent colored areas. An enlarged view of this structure is shown in Fig. 7(b). From this figure and from the related densitogram [see Fig. 7(b) on the right-hand side] it is clear that the spatial resolution (sharpness) of the luminescent pattern is around 1 μ m or better, since 1 μ m coincides with the resolution of the optical microscope used for the image readout. An analysis of the image from Fig. 7(a) shows that such high spatial resolution is reached in the whole area of the image. This result demonstrates a huge ratio between field of view and spatial resolution: (7000:1) \times (2500:1).

It is possible to estimate the resolution limits of the used patterning process by taking into account diffraction and penumbra blurring effects. These effects are the same as for proximity lithography.¹⁵ The penumbra blurring, δ_p , is related to the diameter Φ of the x-ray source, to the gap G between the mask and sample, and to the distance d between the sample and the x-ray source by the formula $\delta_p = \Phi \cdot G/d$. On the other hand, the diffraction blurring, δ_r , due to the wave nature of the incident radiation with wavelength λ , approximately equals $\sqrt{\lambda \cdot G}$. For the typical conditions of the experiments considered here ($\lambda \sim 1-10$ nm, $G \sim 1-10$ μ m, $\Phi \sim 30-300$ μ m, and $d=15$ cm), the expected printing resolution is about 30–300 nm, and limited mainly by the diffraction effect. Due to the low photon energy, the photoelectron blurring can be neglected, according to Ref. 15. To

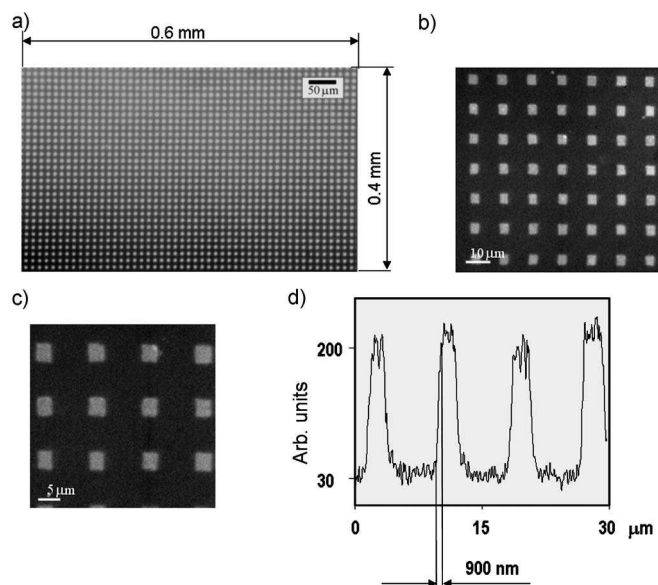


FIG. 8. (a) Image of a 2000 lpi grid placed in contact with a LiF crystal during the exposure to soft x-rays; the LiF is observed with an optical microscope in fluorescence mode with a 20 \times objective; (b), (c) enlarged parts of the 2000 lpi grid image, observed with a Leica confocal microscope with a 40 \times and 100 \times objective, respectively; (d) densitogram of the image showing a submicron spatial resolution.

exclude the possibility that in our experiments the spatial resolution could be decreased by a high penetration of the soft x-ray radiation inside the LiF crystal, the depth of the CCs distribution inside the LiF crystal has been carefully estimated by accurate optical measurement. In our experimental conditions the obtained value for the depth distribution of CCs in the LiF crystals is not exceeding 50 nm.³⁰ All these considerations demonstrate that, in principle, in our experimental conditions, a submicron spatial resolution could be reached, and that the $\sim 1 \mu\text{m}$ spatial resolution that we obtained in Fig. 7 is really limited by the used readout measurement technique, not by the size of the x-ray source or by the spatial resolution of the LiF crystal detector itself. Figures 8 and 9 support this conclusion. These two soft x-ray images have been obtained by using the other laser plasma source, which was a copper tape target irradiated by the Nd glass laser pulses. Two LiF crystals have been placed at 3 cm from the target and masked by a 1000 and by a 2000 lines per inch (lpi) Ni grids. With this source, a single laser shot was sufficient to properly expose the samples. A confocal microscope with a nominal resolution of about 200 nm and working in fluorescence mode has been used to readout the images from the LiF crystals. From the related densitograms of Figs. 8 and 9 it can be clearly seen that a submicron scale spatial resolution is reached. Note again that such detectors deliver images with a submicron resolution in a very wide field of view (up to 7×2.5 mm in our case, but it could be even much larger, when using bigger size LiF crystals or films).

It is also necessary to underline that soft x-ray radiation from laser produced plasma is not the only source that can be used for reaching submicron spatial resolution in LiF imaging detectors. Indeed, submicron luminescent patterns based

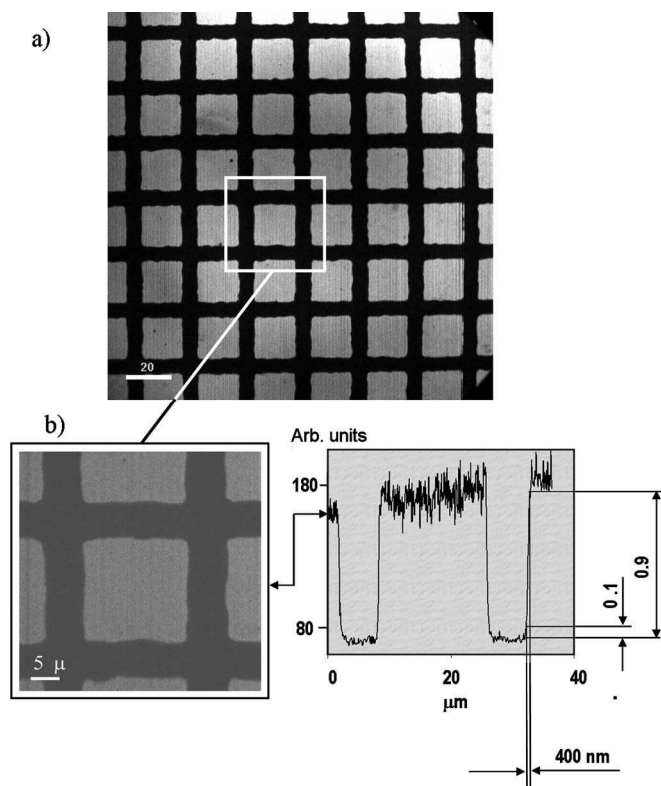


FIG. 9. (a) Image of a 1000 lpi grid placed in contact to a LiF crystal during the exposure to a single shot x-ray radiation emitted by the Nd:glass laser-plasma source with a Cu target, observed with a confocal microscope in fluorescence mode with a 40 \times objective; (b) Enlarged part of the image (a), observed with the same microscope under magnification 100 \times , and densitogram of the image, which shows a submicron spatial resolution.

on CCs in LiF have been obtained also by direct writing processes using a focused x-ray beam with a photon energy of 640 eV provided by the ELETTRA synchrotron facility of Trieste, Italy.³¹ The patterns were produced by scanning the LiF specimen by using a soft x-ray microprobe with a diameter of 100 nm. Luminescent 170 nm wide lines have been obtained on a LiF film³² (in this case a SNOM microscope in fluorescence mode has been used to readout the LiF sample, while the short depth of the film has allowed a coloration depth much smaller than the x-rays penetration length in LiF).

D. Comparison of LiF with other soft-x-ray detectors

Among all soft-x-ray imaging detectors only photoresist (like PMMA, for example) and LiF crystals/films reach a spatial resolution at nanometer scale. So, it is interesting to perform a direct comparison of their response properties in the same experimental conditions.

A very important characteristic of any imaging detector is its dynamic range. So we experimentally compared the dynamic ranges for PMMA and LiF film imaging detectors. Figure 10 shows the results of direct exposure of a PMMA photoresist and a LiF film by using the soft-x-ray radiation emitted by our XeCl laser produced plasma. Both imaging detectors have been placed at 10 cm distance from the LPP source with a copper target and irradiated with 1000 laser pulses, which corresponds to a total fluence of about

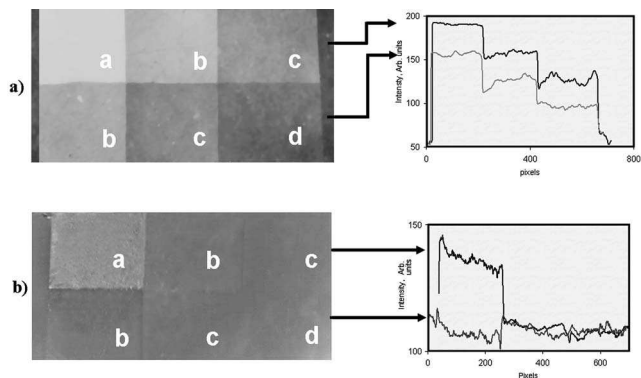


FIG. 10. Result of the exposure of a LiF film (above) and a PMMA photoresist (below) at same irradiance conditions (400 mJ/cm^2) through a step-shaped polypropylene phantom which reduced the x-ray fluence by a factor 1 (area “a”), 150 (area “b”), 300 (area “c”), and 600 (area “d”).

400 mJ/cm^2 . The same step-structure filters (many foils of $1 \mu\text{m}$ thick polypropylene overlapping to form a stair structure) have been mounted in contact to the surface of both detectors. Such filters have reduced the soft x-ray flux density by 150, 300, and 600 times as the polypropylene thickness changes from 1, 2, and $3 \mu\text{m}$ (the first step cuts much more than the following ones just because it eliminates most of the emitted spectrum). From the luminescence images and densitograms in Fig. 10 it is clearly seen that the dynamic range of the LiF film is orders of magnitude wider than that of the PMMA photoresist. In fact, on the LiF film, see Fig. 10(a), the borders of the obtained steps in the image are sharp even in the zones with almost 3 orders of magnitude reduction of the fluence of the soft x-rays (zones C and D), while on the PMMA, see Fig. 10(b), such zones could not be distinguished, nor when analyzed by visible light, neither when analyzed by an atomic force microscope, which is traditionally used for the readout process of developed PMMA. So, the direct comparison clearly demonstrates a big advantage of LiF crystals and films as a submicron imaging detectors compared with traditional PMMA detectors.

We would like also to stress here that from other experiments (for example, from the biological microradiographies on LiF crystals and LiF films) we could clearly see that the dynamic range of LiF detectors is comparable with the dynamic range of the photographic x-ray film, traditionally used for soft-x-ray radiation imaging applications. However, there are still advantages of LiF imaging detectors compared with the photographic films, as reported in the following:

- (i) a much higher spatial resolution (accompanied by a lower sensitivity, of course);
- (ii) the absence of sensitivity to visible and UV light, so that no filtering is required for protecting the detector during the soft-x-ray radiography exposure and readout process;
- (iii) there is not any need of development after the exposure.

In recent years a strong development of so called Image plates for x-ray imaging has been also achieved, and they raised a great interest in different applications, due to higher sensitivity compared with conventional radiographic films.

Somehow, the image plates are similar to the LiF as they are based on the generation of CCs by x-ray exposure on a phosphor plate, and readout process consists of excitation of CCs by He-Ne laser radiation and recording of induced luminescence from each point of the plate.^{33–35} However, there are significant differences between LiF and Image plates. As advantages of the image plate there are both a very high sensitivity (the minimum detectable fluence can be just 10 photons of the 1.5 keV energy, which corresponds to 0.1 nJ/cm^2 , a much smaller value than the one reported here for LiF detectors), and a linear response in a large spectral range. On the other hand the following drawbacks hold:

- (i) the CCs in image plates are not stable with time (the lifetime is of a few hours), and the readout process must be done immediately after the exposure to x ray,
- (ii) during the readout process, image plates are scanned by a narrow (typically in the order of $50\text{--}1000 \mu\text{m}$) He-Ne laser beam, which is time consuming,
- (iii) after reading, the image disappears in the image plates, while in LiF the image is stored permanently,
- (iv) the spatial resolution of the image plates is limited by the grain size of the phosphor structure, of the order of few microns, and depends on the He-Ne reading beam size and, probably, also on thermal diffusion effects,
- (v) the image plates need to be filtered from visible light, so far it was demonstrated that image plates are well suitable for hard x-ray imaging, and it is not yet clear whether they can be efficiently used for EUV radiation imaging.

III. LIF FOR DIFFERENT SOFT-X-RAY IMAGING APPLICATIONS

A. High resolution soft x-ray imaging of biological objects

During the past decade, EUV and soft-x-ray radiation were widely used with contact or projection techniques to image biological samples of different living objects at a spatial resolution around $30\text{--}1000 \text{ nm}$, which is an intermediate case between optical and electron transmission microscope resolutions. Different types of detectors are used for such purposes, but only PMMA photoresists reach a very high spatial resolution, when contact x-ray microradiography is performed. As it has been shown in the previous section, the use of LiF as a detector for soft x-ray submicron imaging could give big advantages compared with the PMMA photoresists. So, here we describe how LiF crystals or films could be used for submicron spatial resolution microradiography of the macro-size biological objects irradiated by soft x-ray radiation generated by laser produced plasma.

Figures 11(a)–11(c) show the images of a dragonfly (*Pyrresoma nymphula*) wing obtained on a LiF film. In this experiment the scheme of Fig. 3(a) with the laser produced plasma source was used. A dried full-size dragonfly wing was mounted on the LiF film surface in full contact. This coupled sample was placed in the vacuum chamber of the “Hercules” (XeCl) laser facility at a distance of 10 cm from

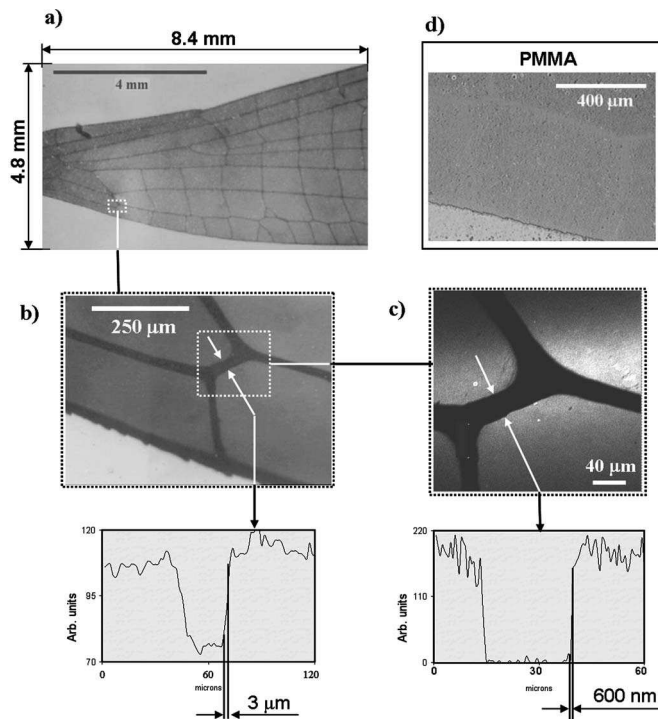


FIG. 11. (a) Image of a *dragonfly* wing obtained on a LiF film and observed under a conventional fluorescence microscope with a $5\times$ objective; (b) and (c) enlarged areas of the image (a), observed under a conventional optical microscope with a $20\times$ objective and under a Leica confocal microscope with a $40\times$ objective, respectively. The densitograms under the images show that the observed spatial resolution is strongly depending from the resolution limit of the used microscope, and that the really reached spatial resolution is not worse than 600 nm . (d) Image of the twin wing (of the same *dragonfly* sample) on a PMMA photoresist, obtained at the same experimental conditions. Note the much poorer dynamical range of PMMA compared with LiF.

the x-ray source (Cu target). The image was generated on the LiF detector with 1100 shots (repetition rate 1 Hz) under an irradiation fluence of $0.4\text{ mJ/cm}^2/\text{pulse}$. After the x-ray irradiation, the colored surface of the LiF film was visualized by different types of conventional and confocal fluorescence microscopes. Under a conventional microscope with a $2\times$ objective, the full size image of the wing is observed, see Fig. 11(a). This figure demonstrates that a small size x-ray plasma source can deliver high contrast images in a very wide field of view. Figures 11(b) and 11(c) show enlarged areas of the same image obtained under a conventional microscope with a $40\times$ objective and under confocal microscope with a $50\times$ objective, respectively. Densitograms of the same detail of the wing rib give a very different spatial resolution of the images: namely, the spatial resolution of the conventional microscope image is in the order of $3\text{ }\mu\text{m}$, while for the confocal microscope image it reaches 600 nm . These figures clearly demonstrate that the spatial resolution limit of the reading fluorescence microscope system plays a crucial role for the analysis of images obtained with LiF detectors. Also, we would like to stress that the wing image has a high-contrast, which is comparable to the one obtained by conventional radiographic films, but with spatial resolution significantly improved.

For completeness, in Fig. 11(d) the optical image of the symmetrical wing of the same *dragonfly*, obtained in the

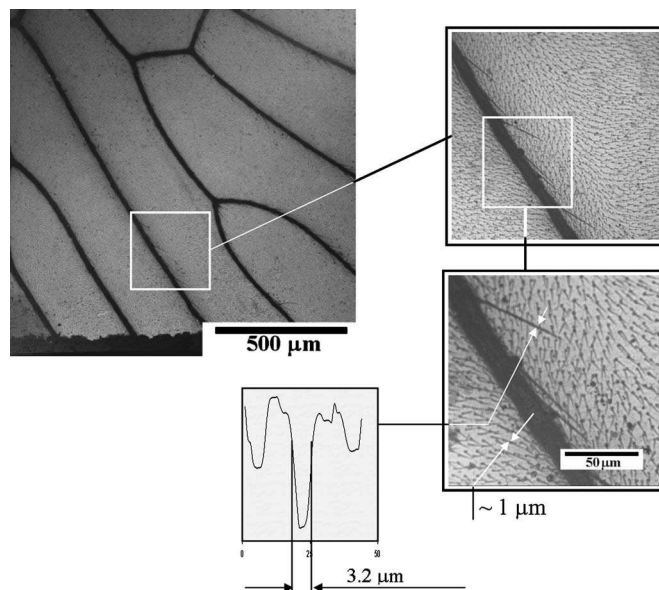


FIG. 12. Image of a *mosquito* wing, obtained by contact radiography on a LiF crystal, and observed under a Zeiss LSM 510 fluorescence confocal optical microscope with a $40\times$ objective with different zooming ratios. The densitogram shows the size of a rib, but the small hairs, which have a thickness $\leq 1\text{ }\mu\text{m}$, are also very well resolved on the whole surface.

same experiment on a developed PMMA photoresist, is presented. In contrast to the image on the LiF film, the image obtained on PMMA has a much smaller contrast, and it is very difficult to distinguish the wing ribs. To underline once more the advantage of the LiF imaging detector compared with PMMA in terms of dynamic range, even by reading this PMMA image by an atomic force microscope, no additional information was obtained.

In Fig. 12 the image of a *mosquito* (*Diptera*) wing, obtained by contact radiography on a LiF crystal with the same laser plasma source is presented. The image has been readout by a Zeiss LSM 510 fluorescence confocal optical microscope with different magnifications. The densitogram shows about $3\text{-}\mu\text{m}$ dimension of the thicker hairs; but also the small hairs, which have a thickness around $1\text{ }\mu\text{m}$, are very well resolved on the whole surface of wing tissue. Such shallow hairs are so thin that they could not be detected by x-ray radiography done on conventional radiographic film.

B. Properties of a capillary discharge x-ray laser beam

High power, short pulse duration, and very small penetration depth of the x-ray laser radiation in LiF, $10\text{--}40\text{ nm}$ for a photon energy of $20\text{--}100\text{ eV}$, allow us to use the LiF detector with a high dose rate and to reach a high spatial resolution. These conditions make LiF a very promising sub-micron detector for x-ray laser beam diagnostics, and for imaging investigations of the spatial parameters of the beam. The LiF based detector can absorb doses orders of magnitude larger than photographic films or CCDs, so that in some cases the laser spot can be imaged without any filters, and hence without any distortion of the intensity and of the phase profiles.

Having in mind such peculiar properties, the LiF detector was successfully used for the investigation of an x-ray

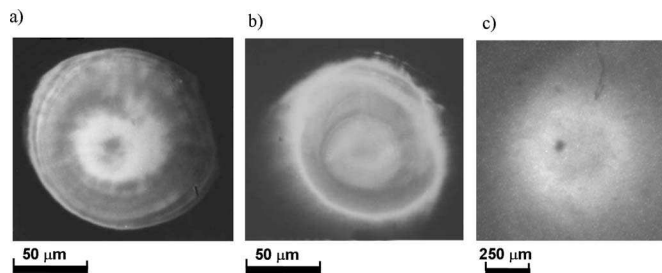


FIG. 13. Observation of the quasi-near-field x-ray laser beam intensity distribution emitted by a Ne-like Ar capillary discharge at $\lambda=46.9$ nm. (a) Conjugate image of the beam at the output of the capillary channel, obtained on a LiF film detector with a demagnification $9\times$ by a focusing multilayer mirror, $f=40$ cm, obtained with a single laser shot for an initial Ar-gas pressure of 0.45 Torr and a 45 cm long capillary. (b) Image of the same laser beam, obtained with the same experimental conditions as in (a), but after shifting the LiF detector by $350\ \mu\text{m}$ out of the mirror conjugate position. The images show changes in the beam intensity distribution at tiny details. (c) A 1:1 conjugate image of the beam profile at the output of the capillary channel, obtained using two 75 cm focal length mirrors and a conventional coupled system composed by CCD+MCP and a phosphor screen.

laser beam at the wavelength 46.9 nm. The experiments were carried at the tabletop capillary discharged x-ray laser facility, developed at the University of L'Aquila, Italy.³⁶ The laser operates on the $3p-3s$ transition of the Ne-like Ar at 46.9 nm (photon energy 26.4 eV). The Ar plasma is excited by a (16–20) kA peak-value, 146 ns long current pulse inside a 3.2 mm diameter, (25–45) cm long alumina capillary, filled with Ar at a pressure of (400–500) mTorr. The laser operates in a highly saturated regime with output energy of 0.3 mJ and pulse duration of 1.7 ns.

Different experiments for the investigation of the x-ray laser beam were performed. Figures 13(a) and 13(b) show the luminescence images of the x-ray laser beam intensity distribution at the output of the capillary channel, recorded on a LiF film. The images were formed by a spherical (40 cm focal length) Sc/Si multilayer mirror placed normally to the capillary axis at 4 m from the laser exit, with a corresponding demagnification $9\times$. No filters were used downstream the laser beam before the detector. As the source diameter is in the order of $300\ \mu\text{m}$, the mirror results to be at few times the Rayleigh distance, so it is almost in the far-field configuration. Consequently, at the best conjugate position [Fig. 13(a)], a demagnified image of the laser quasi-near-field distribution is obtained, and we could very clearly see that, for the used laser parameters (an initial Ar-gas pressure of 0.45 Torr and a 45 cm capillary length), the beam has a very sharp edge and a bright central zone with an annular structure. The high spatial resolution of the detector shows also very tiny details in the intensity distribution. The structure of this intensity distribution is still under analysis and it should be related to the effect on the beam propagation of the plasma density distribution in the discharge.

When the detector has been shifted by $350\ \mu\text{m}$ out of the conjugate position, a slightly defocused image has been obtained as shown in Fig. 13(b), but still the contrast of the image is enough to resolve details of the internal beam structure. Both above images were obtained in a single laser shot. The fluence of the focused monochromatic x-ray radiation on

the surface of the LiF detector was about $100\ \text{mJ}/\text{cm}^2$. The readout process of the images obtained on these LiF films was done by using a Zeiss Axioplan-2 optical microscope in fluorescence mode with an objective $20\times$.

For comparison, Fig. 13(c) shows the image of the quasi-near-field laser beam obtained with a two spherical 75 cm focal length Sc/Si multilayer mirrors with a magnification 1:1 and a conventional high sensitivity detection system composed of a 1392×1040 pixels, $4.65\ \mu\text{m}$ pixel size CCD coupled to a $15\ \mu\text{m}$ pixel size MCP image intensifier and a phosphor screen.³⁷ In this last case it is clear that the structure of the beam is not well resolved, in spite of the absence of the demagnification used in the case of LiF imaging detector. This demonstrates how large the dynamic response and how high the spatial resolution of LiF detector are.

Also a measurement of the x-ray laser beam intensity distribution in the far-field region was done by direct irradiation of a LiF film (that is by unfocused laser radiation). In this case, the detector was placed on the capillary axis at normal incidence of the beam at the distance of 45 cm from the capillary output.

In our case, assuming the beam quality factor M^2 introduced by Siegman³⁸ of about 10 (as expected in a mirrorless laser and also as measured in a similar laser³⁹) and being the Rayleigh distance for a partially coherent beam $Z_R=(\pi/4)\cdot\Phi_S^2/(\lambda\cdot M^2)$ much shorter than 45 cm (where the source size is $\Phi_S\sim 0.3$ mm and the wavelength is $\lambda=46.9$ nm), the obtained image can be considered a quasi-far-field distribution one. In order to cut off the vacuum ultraviolet and most of the soft x-ray spontaneous emission, produced by the laser discharge simultaneously with the lasing, a $0.15\ \mu\text{m}$ thick aluminum filter was used. The filter with its supporting grid (with a thickness of the wires of $60\ \mu\text{m}$, and a period of $360\ \mu\text{m}$) were placed at the distance 8.5 mm in front of the detector to observe the spatial intensity distribution of the laser beam and the shadow image of the grid, simultaneously. The resulting image is shown in Fig. 14. The image was recorded by summing 30 consecutive laser shots with an average fluence of $6.2\ \text{mJ}/\text{cm}^2/\text{shot}$ and then readout by the microscope Zeiss Axioplan-2 in fluorescence mode with an objective $20\times$. In the image of Fig. 14(a), the annular periphery structure of the intensity distribution and the main central lobe are clearly resolved [both in the figure as well as on its densitogram as shown in Fig. 14(b)].

In the same figure, together with the shadow image of the grid, we can clearly distinguish the diffraction patterns, produced by the coherent x-ray laser radiation. These patterns are symmetrical in the vertical and horizontal directions and give very good evidence about the two-dimensional spatial coherence of the laser beam. The origin of this high spatial coherence is well described in Refs. 39 and 41. The high resolution and the high dynamic range of the LiF film allowed to measure the high-spatial frequency oscillations of the diffracted beam intensity, whose period is smaller than $10\ \mu\text{m}$, see the densitograms in Fig. 14(c). In this particular case, where the laser beam was produced through a 25 cm long capillary tube, we could estimate a coherence length in

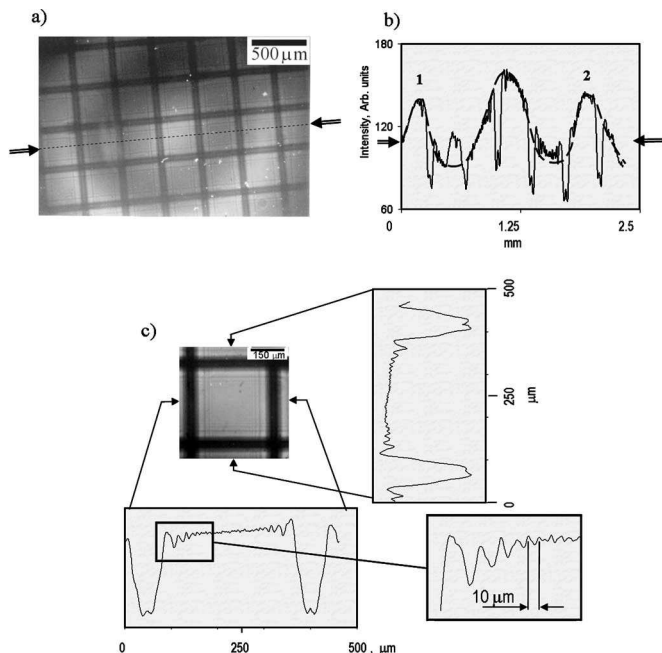


FIG. 14. (a) Observation of the quasi-far-field spatial intensity distribution of the Ne-like Ar capillary discharged x-ray laser beam (circular structure in the image), passing through a $0.15 \mu\text{m}$ Al filter (supported by a Ni mesh) and stored on a LiF film detector placed at a distance of 45 cm from the capillary exit; in the image, the interference patterns generated by the Ni mesh (period $360 \mu\text{m}$, wire thickness $60 \mu\text{m}$) through the 8.5 mm gap between the mesh and the detector are clearly visible (the $500 \mu\text{m}$ bar corresponds to an angle of 1.1 mrad); (b) Densitogram of the image (a); (c) Detail of the patterned image and its densitograms in the two perpendicular directions, showing the 10-micrometer scale oscillation of the intensity due to the diffraction effect.

the order of $200 \mu\text{m}$ at the detection plane. However, a larger coherence length has been found in other experiments performed using longer capillary tubes both by Liu *et al.*³⁹ in a similar Ar laser⁴⁰ and by our group.⁴¹

The high spatial coherence of the x-ray laser allowed to generate fine grating structures with interline distances down to submicron scale, using the Lloyd-mirror interferometric technique. In Fig. 15(a) an image and densitogram of fluorescent patterns with the distance between the maxima and minima of 500 nm, obtained on the LiF crystal, are shown. The image has a very regular structure and a good contrast. In this experiment the Lloyd mirror, which consisted of an 11-cm-long silicon plate with super polished surface, was placed at a distance of 76 cm from the laser capillary output under the grazing angle of 1.09° (19 mrad) between the plane of the mirror and the beam axis [Fig. 15(b)]. To guarantee the largest overlapping area between the direct component of the beam and the reflected one, the LiF was located close to the far edge of the mirror. To obtain a good coloration, the LiF crystal was exposed to ten laser pulses. In these conditions the energy flux on each irradiated area was estimated at $25 \text{ mJ}/\text{cm}^2$ (for more detail see Ref. 42).

IV. CONCLUSIONS

It is demonstrated that EUV and soft-x-radiation efficiently generate CCs in LiF crystals and films, which are optically active and stable at RT. This result allowed devel-

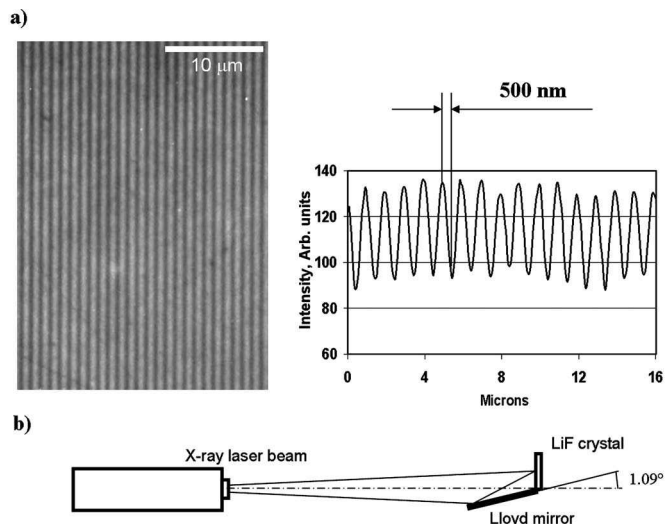


FIG. 15. (a) Image of interference patterns (detail) on LiF and its densitogram. The image was observed with an optical microscope (ZEISS Axioplan 2), operating in fluorescence mode with $100\times$ magnification. Plot profile demonstrates a spatial resolution of 500 nm (limit of the optical microscope). (b) Scheme of the related experimental setup.

oping efficient imaging detectors, in which a high resolution image is encoded in terms of CCs surface density distribution in LiF material. Among the produced CCs, the F_3^+ and F_2 defects have practically spectrally overlapped absorption bands in the blue region, and possess two separated emission bands in the visible spectral range (in the green and in the red region, respectively), so that conventional high-resolution fluorescence microscopy techniques for the readout process can be used.

It is shown that using a pointlike x-ray source, produced by interaction of laser pulses with solid targets as a backlighter, and LiF crystal or film as a detector, it is possible to obtain high spatial resolution, 400–900 nm, images of different test samples or biological objects in a very wide field of view (up to many mm^2). A LiF detector was successfully used also for investigation of an X-ray laser beam intensity distribution in different focusing conditions.

The advantages of the LiF crystal and film imaging detectors in the EUV and soft x-ray spectral range are the following: high spatial resolution, suitable dynamic range, large field of view, small price and rewritable possibility (just by heating the detector to 400°C by a few minutes all CCs recombine), easy managing (no needs of electronic supply, no light protection, vacuum compatible, stable data storage, no development needs, simple readout process). All these features make LiF material a very promising detector for micro-radiography, x-ray contact microscopy, x-ray laser beams diagnostic and other applications, which utilize EUV and soft x-ray radiation.

ACKNOWLEDGMENTS

The authors thank Dr. Marco Ranalli (Policlinico Tor Vergata, Italy) for valuable discussions and Nikon CLSM measurements, Dr. Irmtraud Steinmetz (Leica Mannheim, Germania) for the CLSM images with Leica TC SP2, and are indebted to the Leica and Zeiss Italian staff for their avail-

ability. This work was partially supported by the Italian Project MIUR-FIRB-EUVL (RBNE012ABPB), and also by the Italian Ministry of Foreign Affairs and by the Russian Ministry of Science and Technology in the frame of the Italian-Russian Science and Technology Cooperation Agreement. The work of Dr. T. Pikuz and Dr. A. Faenov was partly supported by a grant from the Italian Ministry of Foreign Affairs through the Landau Network-Centro Volta Fund, and by fellowships granted by ENEA.

- ¹See many articles of Special Issue of Rev. Sci. Instrum. 74 (issue III) (2003).
- ²G. A. Johansson *et al.*, Rev. Sci. Instrum. **73**, 1193 (2002).
- ³C. Tillman *et al.*, J. Opt. Soc. Am. B **13**, 209 (1996).
- ⁴D. Batani *et al.*, Eur. Phys. J. D **21**, 167 (2002).
- ⁵J. Kaiser *et al.*, Eur. Phys. J. D **32**, 113 (2005).
- ⁶B. L. Henke *et al.*, At. Data Nucl. Data Tables **54**, 181 (1993).
- ⁷C. H. Skinner *et al.*, J. Microsc. **159**, 51 (1990).
- ⁸See, for example, review S. M. Gruner, M. W. Tate, and E. F. Eikenberry, Rev. Sci. Instrum. **73**, 2815 (2002).
- ⁹J. H. Schulman and W. D. Compton, *Color Centers in Solids* (Pergamon, Oxford, 1962), p. 221.
- ¹⁰S. K. Sekatskii and V. S. Letokhov, Appl. Phys. B **B63**, 525 (1996).
- ¹¹E. J. Caine and S. D. Miller, J. Vac. Sci. Technol. **16**, 3232 (1998).
- ¹²P. Adam *et al.*, Opt. Express **9**, 353 (2001).
- ¹³G. Baldacchini *et al.*, Opt. Commun. **94**, 139 (1992).
- ¹⁴J. Martin, L. Bischoff, and R. Wannemacher, Opt. Commun. **188**, 119 (2001).
- ¹⁵D. Attwood, *Soft X-Rays and Extreme Ultraviolet Radiation: Principles and Applications* (Cambridge University Press, Cambridge, 1999).
- ¹⁶G. Baldacchini, T. Marolo, R. M. Monteverde, A. Pace, V. S. Kalinov, and A. S. Voitovich, "Annealing of Gamma Rays Colored LiF Crystals," ENEA Report No. RT/2004/FIS/67 (2004).
- ¹⁷E. Sonder and W. A. Sibley, *Point Defects in Solids*, edited by J. H. Crawford and L. M. Slifkin (New York, 1972), Chap. 4.
- ¹⁸F. Seitz, Rev. Mod. Phys. **26**, 7 (1954).
- ¹⁹J. Nahum and D. A. Wiegand, Phys. Rev. **154**, 817 (1967).
- ²⁰G. Baldacchini *et al.*, in *Defects in Insulating Materials*, edited by O. Kanert and J. M. Spaeth (World Scientific, Singapore, 1993), p. 1103.
- ²¹R. M. Monteverde, M. Piccinini, and E. Burattini, Appl. Phys. Lett. **78**, 4082 (2001).
- ²²G. Baldacchini, F. Menchini, and R. M. Monteverde, Radiat. Eff. Defects Solids **156**, 71 (2001).
- ²³S. Bollanti *et al.*, Nuovo Cimento D **20D**, 1685 (1998); see also: Appl. Phys. B, **76**, 277 (2003).
- ²⁴K. B. Fournier *et al.*, Phys. Rev. E **67**, 016402 (2003); J. Phys. B **35**, 3347 (2002).
- ²⁵R. M. Monteverde, in *Handbook of Thin Film Materials*, edited by H. S. Nalwa (Academic, New York, 2002), Vol. 3, Chap. 7, p. 399.
- ²⁶G. Baldacchini *et al.*, J. Phys. Chem. Solids **61**, 21 (2000).
- ²⁷G. Baldacchini *et al.*, Nucl. Instrum. Methods Phys. Res. B **116**, 447 (1996).
- ²⁸*Physics of Color Centers*, edited by W. Beall Folwer (New York and London, 1968), Chap. 2, p. 72.
- ²⁹G. Baldacchini *et al.*, Radiat. Eff. Defects Solids **157**, 569 (2002).
- ³⁰F. Flora *et al.*, Proc. SPIE **5196**, 284 (2004); R. M. Monteverde *et al.*, *ibid.* **5451**, 393 (2004).
- ³¹R. Larciprete *et al.*, Appl. Phys. Lett. **80**, 3862 (2002).
- ³²R. M. Monteverde *et al.*, Phys. Status Solidi C **2**, 298 (2005).
- ³³Y. Amemiya, J. Synchrotron Radiat. **2**, 13 (1995).
- ³⁴M. Thoms, Nucl. Instrum. Methods Phys. Res. A **378**, 598 (1996).
- ³⁵S. G. Gales and C. D. Benlay, in Proceedings of the 28th International Conference on Laser Interaction Matter (ECLIM), Rome, Italy, Sept. 6th–10th, 2004.
- ³⁶G. Tomassetti *et al.*, Eur. Phys. J. D **19**, 73 (2002).
- ³⁷G. Tomassetti *et al.*, Europhys. Lett. **63**, 681 (2003).
- ³⁸A. E. Siegman, Proc. SPIE **1224**, 2 (1990).
- ³⁹Y. Liu *et al.*, Proc. SPIE **4505**, 41 (2001).
- ⁴⁰J. J. Rocca *et al.*, Opt. Lett. **24**, 420 (1999).
- ⁴¹A. Ritucci *et al.*, Phys. Rev. A **70**, 1 (2004).
- ⁴²G. Tomassetti *et al.*, Appl. Phys. Lett. **85**, 4163 (2004).